Research in Astronomy and Astrophysics, 25:035006 (12pp), 2025 March
https://doi.org/10.1088/1674-4527/adb136
CSTR: 32081.14.RAA.adb136

Subpixel-based Bidirectional Distortion Correction for Two-dimensional Astronomical Fiber Spectral Images

Dong-Sheng Hu[1,2], Chuan-Qi Chen[1,2], Hao-Jie Yang[1,2], An-Zhi Wang[1,2], Gang Yue[1,2], Zhao-Xv Gan[1,2], Xu-Dong Chen[1,2], Yun-Xiang Yan[1,2,3], Yue Zhong[4], Zhi Xu[4], Zhong-Quan Qu[4], Peng-Fei Wang[1,2,3], Tao Geng[1,2], Shuang Chen[5], and Wei-Min Sun[1,2]

[1] Key Laboratory of Photonic Materials and Devices Physics for Oceanic Applications, Ministry of Industry and Information Technology of China, College of Physics and Optoelectronic Engineering, Harbin Engineering University, Harbin 150001, China; sunweimin@hrbeu.edu.cn
[2] Key Laboratory of In-Fiber Integrated Optics of Ministry of Education, College of Physics and Optoelectronic Engineering, Harbin Engineering University, Harbin 150001, China
[3] Qingdao Innovation and Development Center of Harbin Engineering University, Qingdao 266000, China
[4] Yunnan Observatory of Chinese Academy of Sciences, Kunming 650011, China
[5] State Key Laboratory of Aerodynamics, China Aerodynamics Research and Development Center, Mianyang 621000, China
Received 2024 July 1; revised 2024 December 19; accepted 2025 January 29; published 2025 March 5

Abstract

This paper proposes a subpixel transformation method to correct Keystone and Smile distortions in fiber spectral images from the Fiber Arrayed Solar Optical Telescope. These distortions affect the spatial and spectral positions, degrading resolution and accuracy. To correct Keystone distortion, we use a local summation and peak-finding method to locate central horizontal coordinates, calculate shifting values, and straighten the curves. For Smile distortion, we use quartic polynomial fitting based on absorption lines at different wavelengths. This technique preserves subpixel components, redistributes pixel values, and interpolates non-fiber portions, rectifying the spectra for accurate analysis. The method can also be applied to other astronomical projects like Large Sky Area Multi-Object Fiber Spectroscopic Telescope, enhancing the accuracy and reliability of spectral data in various astronomical studies.

Key words: techniques: miscellaneous – techniques: image processing – techniques: spectroscopic – methods: miscellaneous

1. Introduction

Fiber integral field units and multi-object fiber spectrographs are widely used in astronomical observations. These instruments, such as the Fiber Arrayed Solar Optical Telescope (FASOT; Qu 2011), the Large Sky Area Multi-Object Fiber Spectroscopic Telescope (LAMOST; Cui et al. 2012), the AAOmega multi-object fiber spectrograph (Lidman et al. 2020), and the Sloan Digital Sky Survey (Infante-Sainz et al. 2020), use multiple fibers to channel light from celestial objects into a spectrograph, allowing simultaneous acquisition of spectral data from numerous targets (Smee et al. 2013; Ozaki et al. 2020; Bai et al. 2021; Böker et al. 2022). Their spectrometers commonly image the fiber outputs onto CCD or CMOS detectors. After dispersing by gratings, the fiber output images are spread out by wavelength along the spectral direction. Due to the large field of view of these spectrographs, the resulting two-dimensional fiber spectral images often exhibit varying degrees of distortion after dispersion and imaging by the spectrometer's optical elements. These distortions are typically categorized into Keystone distortion and Smile distortion (Leung et al. 2022). In the unprocessed fiber spectral images, an individual fiber spectrum exhibits a distortion relative to the pixel column, causing spectral lines along the pixel column to converge or diverge toward a single point, resembling the "Keystone" shape seen in architecture, hence termed Keystone distortion. Conversely, Smile distortion in the overall spectra appears as an arc resembling a smile across a certain absorption line of all fiber spectra. Keystone distortion results in spectral signals of the same wavelength showing different intensities at different spatial positions. Smile distortion causes the signals of the same wavelength from different fibers not to align spatially. Both distortions can affect wavelength correction and the geometric integrity of the spectral images, leading to reduced spectral resolution and inaccuracies in the identification and quantitative analysis of spectral lines. The FASOT solar spectrum data used in this paper are from the spectrograph at the Lijiang Observatory, with the absorption lines typically representing characteristic lines from the solar spectrum. The imaging system has a focal length of 642.84 mm; grating specifications are 830 lines mm^{-1}, order $m = 2$; the grating incidence angle is $37.^{\circ}44$, and each pixel corresponds to 3.76 μm. The core diameter of the fiber is approximately 35 μm, and the spacing between two adjacent fibers is about 130 μm. Figure 1(a) and

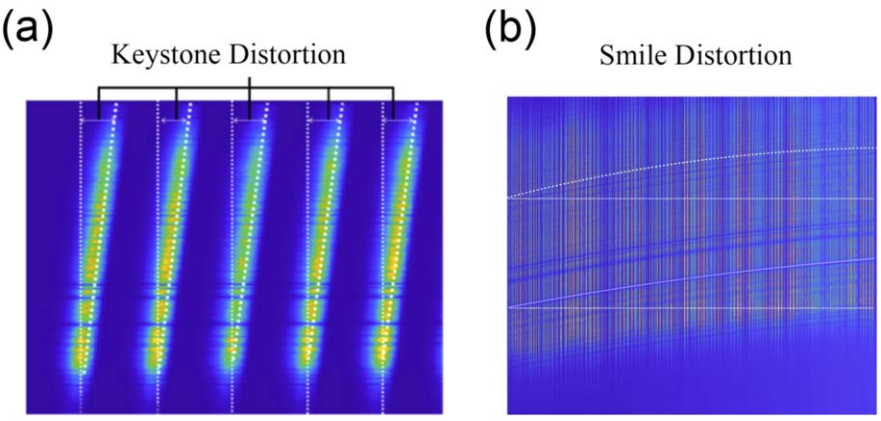

Figure 1. Two types of distortions in fiber spectral images. (a) Keystone distortion. (b) Smile distortion.

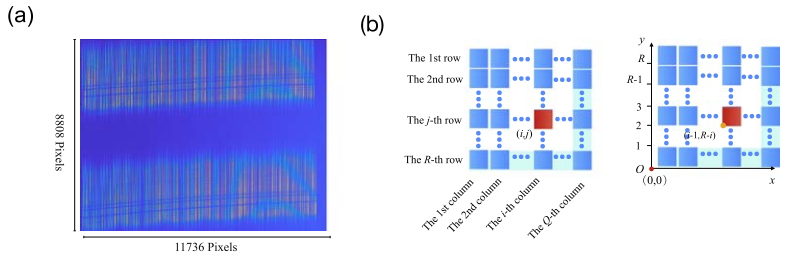

Figure 2. Diagram of matrix parameter definition for the fiber spectrum image. (a) FASOT fiber spectroscopic image. (b) Schematic of the spectrum image matrix.

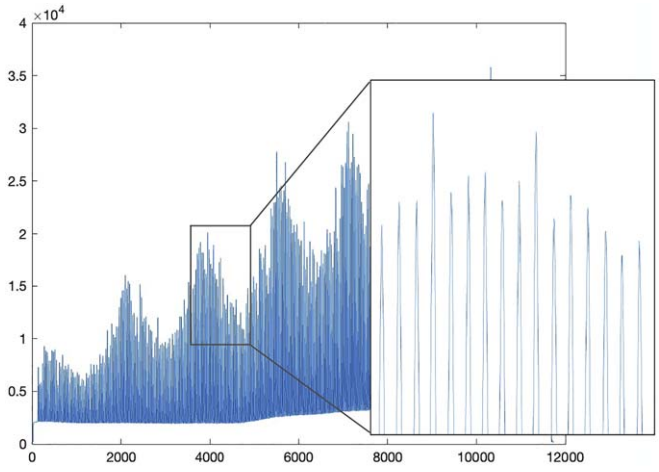

Figure 3. Result of accumulated pixel values from row 71 to row 80. We sum the pixel values of rows 71–80 in the fiber optic spectrum image to verify the peak-finding algorithm.

(b) illustrates the Keystone and Smile distortions present in the FASOT spectrum, respectively.

To process deformed fiber spectra, the common approach involves separating the spectrum of a single fiber and applying mapping and interpolation for correction. Zhang et al. proposed and verified a method using an off-axis lens to correct Smile and Keystone distortions through simulation (Zhang et al. 2022). Koloniatis et al. introduced a Smile correction method based on trend lines, utilizing two criteria for spectral Smile quantification without relying on a radiative transfer model (Koloniatis et al. 2020). Hong et al. developed an image field identifier that separates images by field and wavelength, performs multiple calculations for Smile and Keystone distortions, and corrects spectra by shifting pixels (Hong et al. 2017). Leung et al. employed K-means clustering to accurately identify and correct curved spectral lines in real-time spectral images (Leung et al. 2022). Johnson et al. addressed Smile distortion by incorporating a calculated amount of positive distortion into the optical design, counteracting its effects (Johnson et al. 2020). Generally, traditional correction methods avoid altering spectra during data acquisition to preserve the original spectral information as much as possible.

In practical applications, the essence of a fiber spectrum is the superposition of the dispersive image of this fiber end at different wavelengths on the CCD surface. Different coupling conditions at the telescope's incident end would cause different output profiles of the fibers, which could affect the spectral resolution. To further optimize spectral analysis, we aim to analyze the impact of energy distribution at the fiber output on spectral resolution. This requires obtaining the intensity

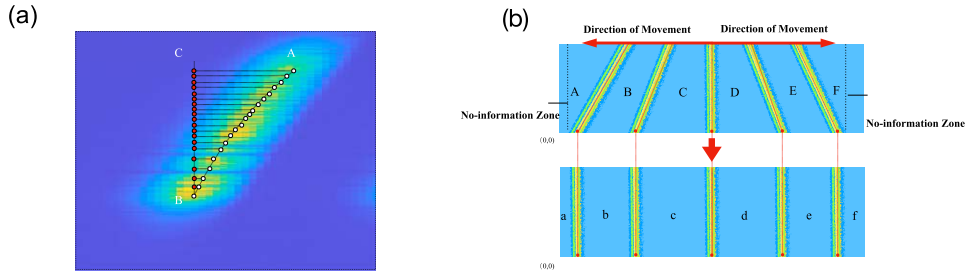

Figure 4. Schematic of correction principles for Keystone distortion. (a) Horizontal movement of peak centers in fiber spectrum image during Keystone distortion correction. (b) The overall change in fiber spectrum morphology before and after correction.

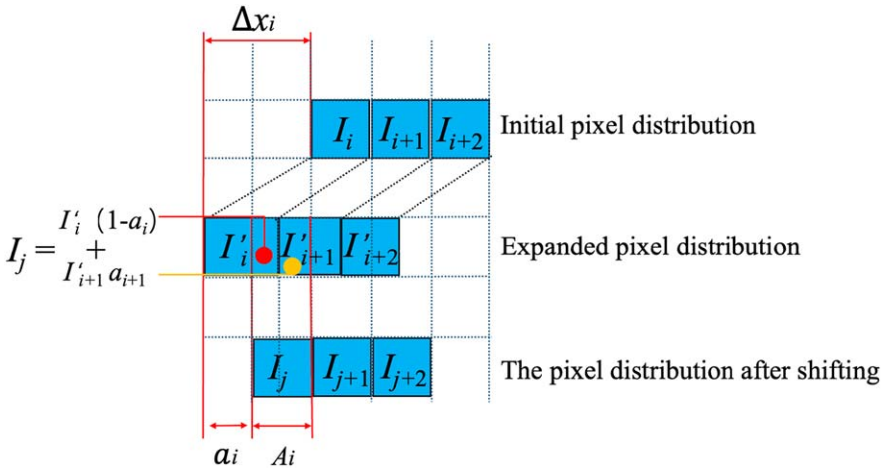

Figure 5. Diagram of Keystone distortion correction principle

Table 1
Definition of Parameters in Equation (2)

Parameter	Definition
x_m, x_{m+1}	The horizontal coordinates of the peak centers for the mth and $(m+1)$th fiber spectra.
Δx_m, Δx_{m+1}	The displacement of the peak centers for the mth and $(m+1)$th fiber spectra.
x_i	The horizontal coordinates of the ith pixel between the mth and $(m+1)$th fiber peaks.
Δx_i	The displacement of the ith pixel.

distribution at the fiber output by superimposing intensities of different wavelengths. To ensure the rationality of the superposition, the spectra must first be straightened without diIn this study, we propose a subpixel transformation method to correct Keystone and Smile distortions in two-dimensional fiber spectral images. During the correction process, we preserve the subpixel components of the fiber spectra, redistribute the pixel values of each point using weighting factors, and interpolate the non-fiber spectral portions. We sum the processed fiber spectra along the dispersion direction, providing data support for obtaining the fiber output end.

2. Principle of Correction

2.1. Matrix Parameter Definition of the Fiber Spectrum Image

In this study, we utilized the fiber spectral image from FASOT, depicted in Figure 2(a). This image contains a spectrum of two

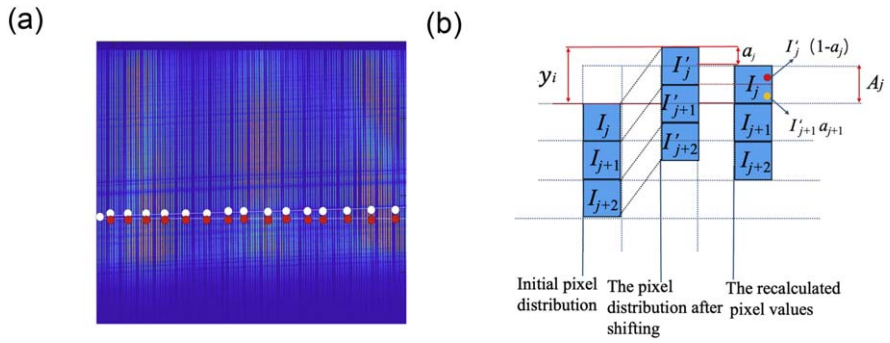

Figure 6. Principle of Smile distortion correction. (a) The vertical movement of the peak centers in the fiber spectrum image during Smile distortion correction. (b) Schematic diagram of the correction principle.

Table 2
X-coordinate of the Spectral Center of Some Optical Fibers

Row Number	1st Fiber	80th Fiber	160th Fiber	240th Fiber	320th Fiber
10	98	2879	5557	7823	11057
20	97	2877	5557	7823	11057
30	95	2877	5556	7822	11058
2000	82	2867	5556	7825	11069
2010	81	2867	5556	7825	11069
2020	81	2865	5553	7825	11069
4480	78	2855	5553	7828	11082
4490	77	2855	5552	7829	11082
4500	75	2854	5552	7829	11082

Table 3
The Pixel Movement of Some Fiber Spectra in a Particular Row

Row Number	1st Fiber	80th Fiber	160th Fiber	240th Fiber	320th Fiber
10	17.35	2.25	3.70	22.66	24.79
20	17.13	2.13	3.58	22.49	22.49
30	16.86	1.97	3.43	22.37	22.37
2000	9.73	1.86	2.65	10.75	10.75
2010	9.58	1.74	2.41	10.47	10.47
2020	9.39	0.77	2.18	10.22	10.22
4480	0.28	0.35	0.76	0.58	0.58
4490	0.12	0.09	0.34	0.27	0.27
4500	0.00	0.00	0.00	0.00	0.00

slits, and each slit generates fiber spectra with a horizontal length of 11,736 pixels. Vertically, the spectra from the upper and lower slits are 4500 and 4308 pixels, respectively. Our analysis focused on processing the upper half of this fiber spectral image. Figure 2(b) illustrates how to describe the position of any element within the matrix. We establish a coordinate system with the bottom-left corner of the bottom-left pixel of the image (i.e., the first column and last row of the fiber spectrum matrix) as the origin, where x and y represent the distribution direction of the fiber alignment and the wavelength dispersion, respectively. The unit of both coordinates is one pixel. Both x and y are measured in pixels. Since the row indices of the matrix increase from top to bottom, the central coordinates of the pixel in the jth column and jth row are $(i-1, R-j)$, where R is the total number of rows in the spectrum matrix. Thus, the image in Figure 2(a) forms an 11,736 × 8808 matrix. For convenience, this paper focuses on the upper half, resulting in a matrix size of 11,736 × 4500.

This addition clarifies the coordinate system and matrix parameters used in the study.

2.2. The Principle of Correction of Keystone Distortion

2.2.1. Finding the Central Peak Coordinates

From Figure 2, each fiber spectrum has a central peak, stortion.

which represents the spectrum's midpoint. Local summation of ten rows and peak-finding approach for feature extraction were used to reduce the influence of noises. The initial peaks of each spectrum were identified corresponding to different wavelengths. The x-axis in Figure 3 represents the horizontal coordinates of the elements in the fiber spectrum matrix, while the y-axis represents the summed values of the elements from rows 71 to 80. The x-coordinate of the peak in the figure corresponds to the central horizontal coordinate of the elements in row 75 of the fiber spectrum matrix. The positions of each peak correspond one-to-one with the actual fiber spectra, which demonstrates the reliability of the method.

By performing the above operation on all rows of the fiber spectrum image matrix, the data points representing the central coordinates of each fiber spectrum can be obtained. We fit the data points with a quartic function, as given in Equation (1).

$$x = Ay^4 + By^3 + Cy^2 + Dy + E. \quad (1)$$

Here, the coefficients A, B, C, D, and E are constants to be determined. Using Equation (1), the x-coordinate values for each fiber spectrum at all y-values can be calculated.

Table 4
The Shifting Pixel of the Values of the Four Absorption Lines from Columns 1000 to 10000

The Sequence Numbers of the Absorption Lines	Column 1000	Column 3000	Column 5000	Column 7000	Column 9000	Column 11000
1	44.79	124.35	124.71	202.33	337.83	414.02
2	44.77	124.37	124.64	202.29	337.85	413.99
3	44.81	124.35	124.73	202.33	337.82	414.03
4	44.77	124.32	124.69	202.31	337.83	413.97

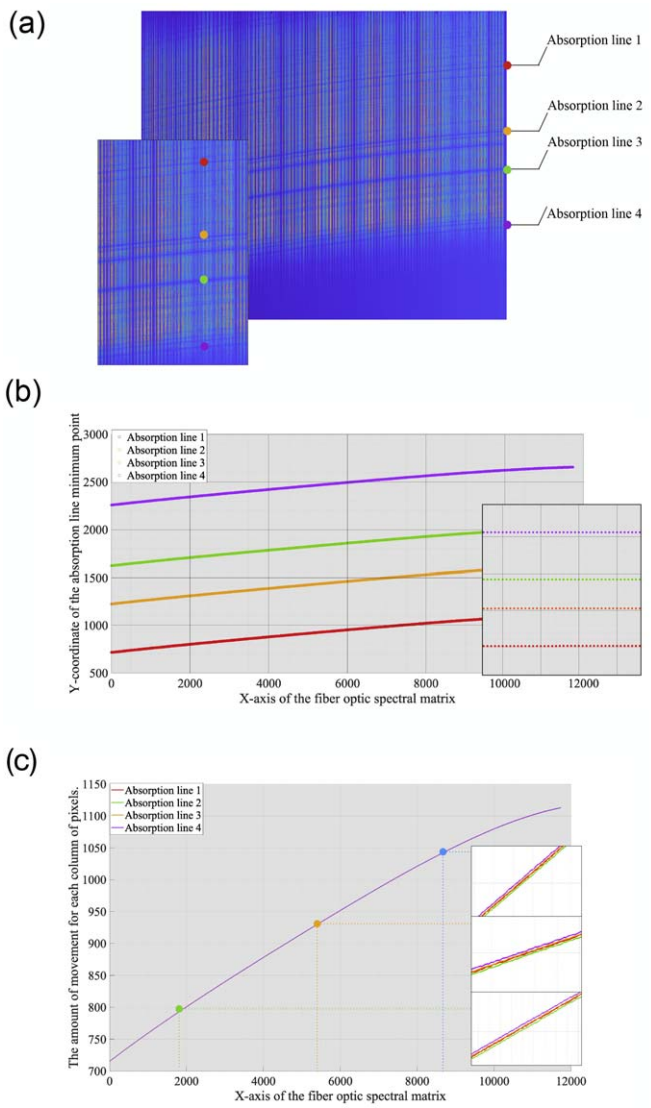

Figure 7. The four selective absorption lines and their pixel shifts. (a) A schematic diagram of the four selected absorption spectral lines. (b) The fitted curve of the valley points for the four absorption lines. (c) A partial monitoring schematic diagram of the pixel offsets for the four absorption lines

2.2.2. Movement of Central Peak Pixels

For each fiber spectrum, the x-coordinate of the bottommost row is used as the reference, and the central positions of peaks of the other rows are adjusted accordingly. Figure 4(a) shows the horizontal movement of fiber spectrum peak centers during Keystone distortion correction. White curve AB represents the peak positions, while red line CB shows the corrected theoretical positions. Figure 4(b) illustrates the overall change in fiber spectrum morphology before and after correction. In the figure, the red dots represent the central peaks of the bottommost fiber spectra. Fiber spectra on either side of the centerline are moved according to the directions indicated by the red arrows. The areas between the fiber spectra, from region A to region F, are expanded to regions a to f respectively. Since the left and right boundaries of the fiber spectrum matrix do not align with the farthest points of the fiber spectra on either side, the pixels in regions A and F are still expanded, preserving information beyond the outer fiber spectra. The central peak coordinates of each fiber spectrum remain aligned, while the non-peak pixels are stretched. This stretching reduces the values of individual matrix elements, but the overall sum of the element values remains unchanged, meaning the total pixel value of the fiber optic spectrum is conserved, and total energy remains constant.

2.2.3. Movement of Non-peak Pixels

For the non-peak pixel sections, we take the pixel values of a specific row between the mth and $(m+1)$th fiber spectra as an example for discussion. By performing linear interpolation on the pixel values of the middle section, the pixel displacement for the ith column should satisfy Equation (2), where the meaning of each parameter is shown in Table 1.

$$\frac{x_i - \Delta x_m}{x_{m+1} - x_m} = \frac{(x_i + \Delta x_i) - (x_m - \Delta x_m)}{(x_{m+1} + \Delta x_{m+1}) - (x_m + \Delta x_m)}. \quad (2)$$

Since i in the fiber spectrum matrix represents the column index of the matrix element, variable substitution can be applied using Equation (3), which leads to Equation (4).

$$x_i = i - 1, \quad (3)$$

$$\frac{i - 1 - \Delta x_m}{x_{m+1} - x_m} = \frac{(\Delta x_i + i - 1) - (x_m + \Delta x_m)}{(x_{m+1} + \Delta x_{m+1}) - (x_m + \Delta x_m)}. \quad (4)$$

After simplification, we obtain

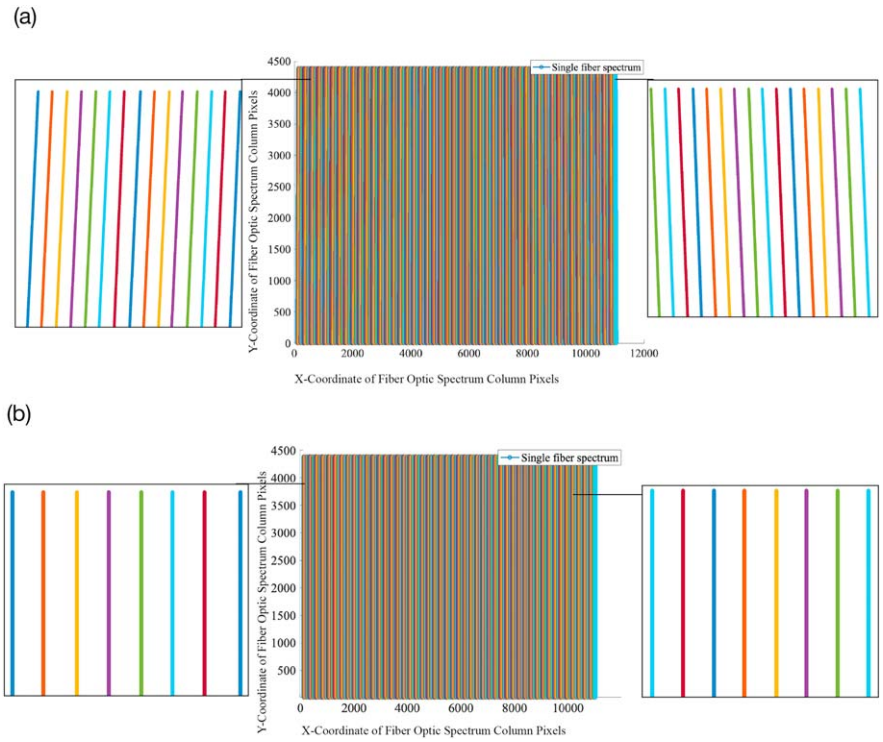

Figure 8. Distribution of fiber optic spectra before and after Keystone correction. (a) Fiber optic spectrum distribution before correction. (b) Fiber optic spectrum distribution after correction.

Table 5
Statistical Results of the Fitting Difference in Pixels of the *x*-coordinate of the Fiber Spectrum Centers

Range of Pixel Differences	The Number of Points in the Interval	Percentage
0.00–0.10	1317555	87.40%
0.11–0.20	83671	5.55%
0.21–0.30	52653	3.49%
0.31–0.40	42164	2.80%
0.40–0.42	11457	0.76%

Equation (5) can be used to calculate the displacement of any non-peak pixel position to correct for Keystone distortion.

2.2.4. The Principle of Value Reassignment of Keystone Distortion

During matrix processing, adjustments are made in integer pixel movement and subpixel movement through a "weighted assignment." The principle of subpixel transformation is shown in Figure 5. In Figure 5, the first row of squares represents the pixels before correction, the second row represents the expanded pixels, and the third row represents the pixels reassigned due to the constraints of the pixel grid. We analyze the pixels in the *i*th, (*i*+1)th, and (*i*+2)th columns of one row in the fiber spectrum matrix. Let their initial pixel values be I_i, I_{i+1}, and I_{i+2}. After expansion, the pixel values become $I_i^{'}$, $I_{i+1}^{'}$, and $I_{i+2}^{'}$. According to the explanation in Section 2.2.2, the

$$\Delta x_i = \frac{(i-1-\Delta x_m)(x_{m+1}-x_m-\Delta x_{m+1}+\Delta x_m)+(i-1)(x_{m+1}-x_m)-x_m(x_{m+1}-x_m)}{x_{m+1}-x_m}. \quad (5)$$

For the regions beyond the leftmost fiber spectra ($i < x_1$), the data from the 1st and 2nd fiber spectra are used for extrapolation. For the regions beyond the rightmost fiber spectra ($i > N$), the data from the ($N-1$)th and Nth fiber spectra are used for extrapolation, where N represents the total number of fiber spectra.

Table 6
Statistics of the Fitting Difference in Pixels of the Absorption Lines

Absorption Line	The Difference in Position 0.00–0.10	The Difference in Position 0.11–0.20	The Difference in Position 0.21–0.30	The Difference in Position 0.31–0.40	The Difference in Position 0.40–0.45
1	77.35%	9.47%	7.56%	4.79%	0.83%
2	83.38%	8.70%	4.16%	3.31%	0.15%
3	79.96%	6.65%	8.80%	3.78%	0.81%
4	80.15%	8.22%	6.71%	3.95%	0.97%

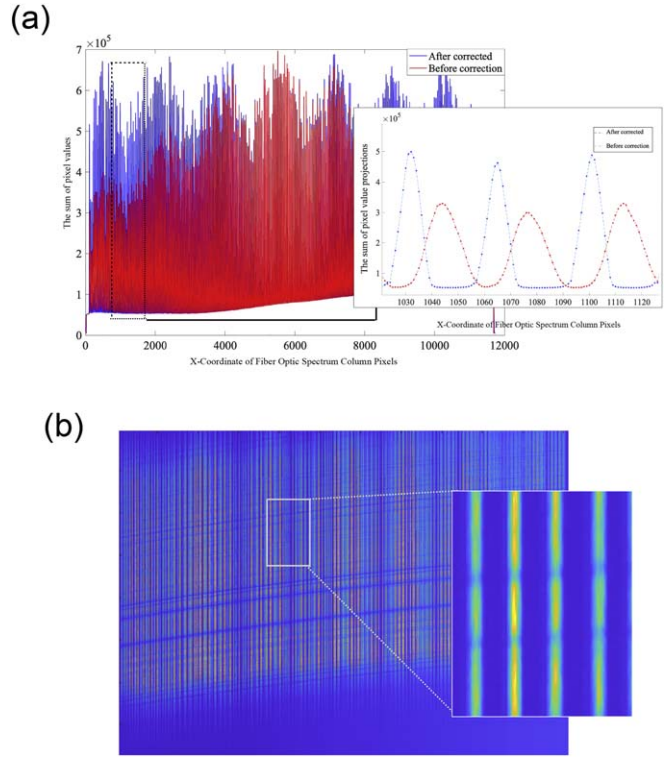

Figure 9. Projection analysis of Keystone distortion. (a) The projection diagram of the fiber optic spectrum and its partially magnified schematic. (b) Spectrum after Keystone distortion correction and partial magnified view.

pixel values before and after transformation satisfy Equation (6), where k_i is the expansion factor for the pixel value in the ith column of the selected row, and $k_i > 1$.

$$I_i^{'} = \frac{Ii}{k_i}. \tag{6}$$

If we disregard the pixel shape changes caused by expansion, the initial pixel should extend along the x-axis, as shown in the transition from the first row to the second row in Figure 5. The difference in the horizontal coordinates of the left boundaries between the two rows should be the movement amount Δx_i for the ith pixel in the selected row, as shown in Equation (7), where A_i and a_i are the integer and fractional parts, respectively. The element value of the new pixel is determined by the two consecutive pixels, as shown in Equation (8) and Figure 5.

$$\Delta x_i = A_i + a_i, \quad k_i = \Delta x_i - \Delta x_{i-1}, \tag{7}$$

$$I_i^{'} = \frac{I_i}{k_i}(1 - a_i) + \frac{I_{i+1}}{k_{i+1}}a_{i+1}. \tag{8}$$

2.2.5. The Principle of Correction of Smile Distortion

Smile distortion was corrected after Keystone correction. The pixel values of 17 columns, the approximate width of a fiber spectrum, were averaged to replace the intensities of the corrected peaks. Then a valley-finding approach was used at different parts of each fiber spectrum. Four valleys were chosen to determine the correction factors. Their y coordinates were fit to a quartic polynomial function of the x coordinates as written in Equation (9).

$$y = Fx^4 + Gx^3 + Hx^2 + Ix + J. \tag{9}$$

Here, the coefficients F, G, H, I, and J are another set of constants to be determined. The coordinate of the leftmost fiber of a valley was chosen as the reference. All other valleys were shifted to align with the reference as Figure 6(a). The white dots in Figure 6(a) represent the center positions of the same absorption line for each fiber spectrum, determined by the valley-finding algorithm. The red dots indicate the corrected positions of the corresponding absorption lines, with all the red dots having consistent vertical coordinates. Through calculation, the number of coordinate points obtained is equal to the total number of fiber spectra, N. By performing a quartic fitting on these data points, the pixel movement for each column of the fiber spectrum matrix can be determined. Figure 6(b) illustrates this movement. Let the pixel values in a certain column for rows j, $j + 1$, and $j + 2$ be denoted as I_j, I_{j+1} and I_{j+2}, respectively, and the vertical movement for the jth pixels in this column is denoted as Δy_j.

Following the approach of Equations (3) and Equations (4), the overall movement can be expressed as

$$\Delta y_j = A_j + a_j. \tag{10}$$

The values A_j and a_j represent the integer and fractional parts of the movement, respectively. The pixel value in row j of the

Table 7
The Pixel Values Required to Shift the Pixels from Columns 1000 to 10000 for the Absorption Lines 5, 6, and 1

The Sequence Number of the Absorption Lines	Column 1000	Column 3000	Column 5000	Column 7000	Column 9000	Column 11000
1	44.79	124.35	124.71	202.33	337.83	414.02
5	44.79	124.33	124.70	202.32	337.84	414.00
6	44.80	124.35	124.68	202.32	337.82	413.99

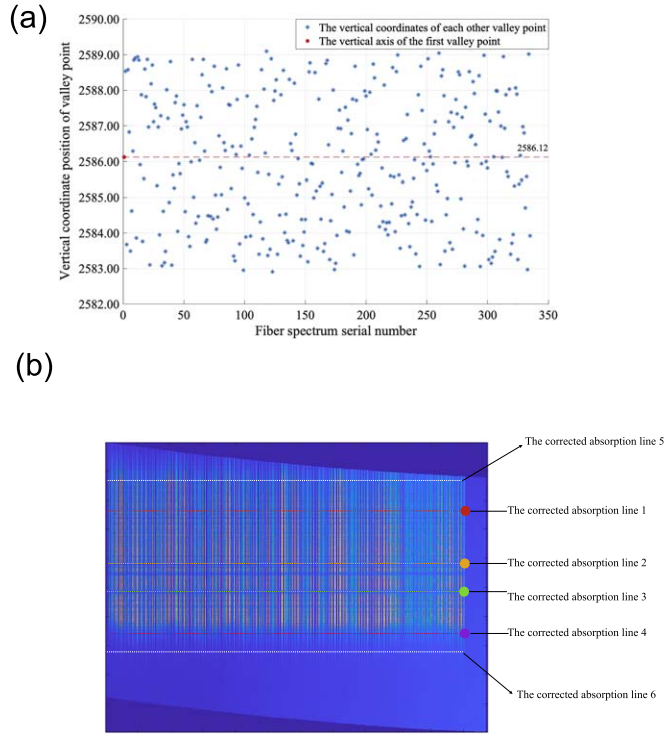

Figure 10. Results after Smile distortion correction. (a) Fluctuation distribution of the center peak ordinates for the same absorption line across different fiber spectra. (b) Appearance of the four fiber spectrum lines after Smile distortion correction.

selected column is

$$I_j^{'} = I_j(1 - a_j) + I_{j+1}a_{j+1}. \quad (11)$$

At this point, both types of distortion have been corrected. For the FASOT spectrum, all valleys have the same movement, so there is no expansion factor for smile distortion.

3. Correction Process

3.1. Correcting Keystone Distortion

We corrected the Keystone distortion according to the above principle. This process involved (1) using the local addition and peak finding algorithm to find the x-coordinates of the spectral center of each fiber every 10 rows, (2) determining the x-coordinates of the fiber spectral center for each row based on quartic polynomial function fitting, (3) correcting peak positions to align peaks to a vertical line, and (4) aligning other pixels in the spectrum based on linear interpolation and extrapolation.

As shown in Table 2, the x-coordinates of the spectral center of each 10 rows of fiber spectrum for the 1st, 80th, 160th, 240th, and 320th fibers are listed, with the last column being the selected ordinate. From the table, it can be observed that the change in the x-coordinate of the spectral center was more pronounced when the difference in the number of rows was larger, which proved that there was a Keystone distortion in the fiber spectrum.

After the quartic polynomial function fitting, the optical fiber spectrum has a definite center coordinate on each row, and the pixel that needs to be moved can be determined by calculating the difference between the coordinates of the center point of any row and the coordinates of the center point of the last row. Table 3 shows the number of pixels that need to be moved in a particular row of the partial fiber spectrum.

3.2. Correcting Smile Distortion

We corrected Smile distortion with a similar approach. First, four absorption lines were selected for analysis in different bands, as shown in Figure 7(a). To facilitate observation, the selected absorption line section in Figure 7(a) has been enlarged. The absorption lines marked in the same color represent the same line. The coordinates of the valley points were found using the same peak finding method and quartic polynomial function fitting method as in Figure 7(b). We used the vertical axis of the leftmost absorption line as a reference to calculate the amount of pixel shift needed for all other columns. Figure 7(c) shows the variation trend of the pixel shift required for each column caused by four different absorption lines. Three areas were selected in the image for magnification. Table 4 lists the pixel values required to shift the pixels from columns 1000 to 11,000 for four absorption lines, with a statistical interval of 2000 columns. The first row represents the column numbers, the first column represents the selected absorption line numbers, and the data in the table indicate the pixel displacement for each column in the specified absorption line.

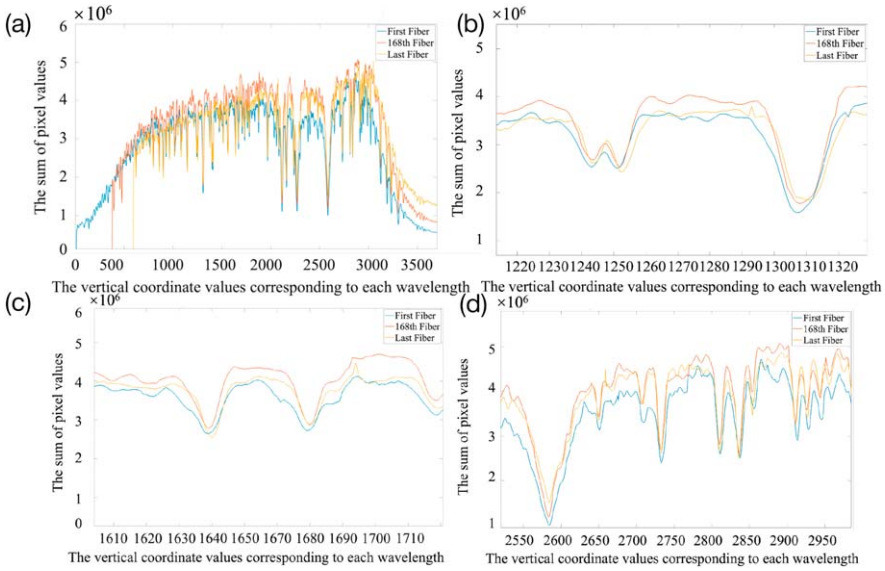

Figure 11. A diagram illustrating the wavelength fluctuations after correction for the 1st, 168th, and 335th fiber spectra. (a) The results of summing along the wavelength direction for the selected 1st, 168th, and 335th fiber spectra. (b) Wavelength fluctuations for the band corresponding to the pixel range of 1220–1320. (c) Wavelength fluctuations for the band corresponding to the pixel range of 1610–1710. (d) Wavelength fluctuations for the band corresponding to the pixel range of 2550–2950.

From Figure 7(c) and Table 4, we found that the shift values of the four absorption lines were almost the same. Therefore, it is reasonable that we chose one of the quartic polynomial functions to calculate the shift values of all spectra.

4. Verification of the Correction Effect

4.1. Correction Effect of Keystone Distortion

We still use the method of local addition and peak finding every 10 lines of pixels, as well as the method of quartic polynomial fitting, to find the x-coordinate position of the corrected optical fiber spectral center. The fiber spectral center distribution is shown in Figure 8(a) and (b). The horizontal axis of Figure 8(a) and (b) represents the x-coordinate of the column pixels in the fiber spectrum image, while the vertical axis represents the y-coordinate of the row pixels in the fiber spectrum image. Each line corresponds to a fiber spectrum, and we have magnified certain sections of the fiber spectra. Figure 8(a) and (b) shows the overall shape changes before and after fiber spectrum correction respectively. This change is mathematically characterized by whether the x-coordinates of the peak centers of each fiber spectrum are consistent before and after correction. We assess the effectiveness of Keystone distortion correction by analyzing the distribution of x-coordinate differences between the peak centers of the same fiber spectrum before and after correction, as well as performing a longitudinal summation of the elements in each fiber spectrum.

After calculation, the x-coordinate difference between the fiber spectral centers before and after correction reached as high as 24.79 pixels. The value is of the same order of magnitude as the horizontal pixel range of the actual processed FASOT fiber optic spectra, so the spectral line curvature caused by Keystone distortion cannot be ignored. The distribution of x-coordinate differences for the peak centers of some fiber spectra are displayed in Table 5. Table 5 shows that the maximum pixel deviation in the corrected image is 0.42 pixels. Over 87.40% of spectral centers deviate from the fitting fourth power exponent by no more than 0.10 pixels, while only 0.76% exceed a 0.40 pixel deviation. The larger deviations are mainly at the image edges where contrast is lower, but all deviations remain within 0.50 pixels.

To analyze intensity changes across wavelengths before and after correction, we vertically summed all pixels in the fiber optic spectrum matrix to obtain the horizontal projection, as shown in Figure 9(a). The projection resembles a Gaussian function, where the bandwidth is defined as the function's width and the pixels between two fiber spectra as the background. After correction, the peaks of different wavelengths were aligned as demonstrated in Figure 9(b). The sum of a fiber spectrum represents the profile shape of this fiber output. The ranges of the spectrum and the background fit well to the fiber setup of the pseudo slit.

The error in this method arises from the expansion factor k_i defined in Section 2.2.3. Since k_i is based on the difference in the horizontal coordinates of the fiber spectrum's center peak, inaccuracies in identifying the peak position can distort pixel value calculations after expansion. The method outlined in Section 2.2.1 effectively resolves this issue. In subsequent corrections, because the equations for linear interpolation and extrapolation are fixed, the movement of each pixel and its

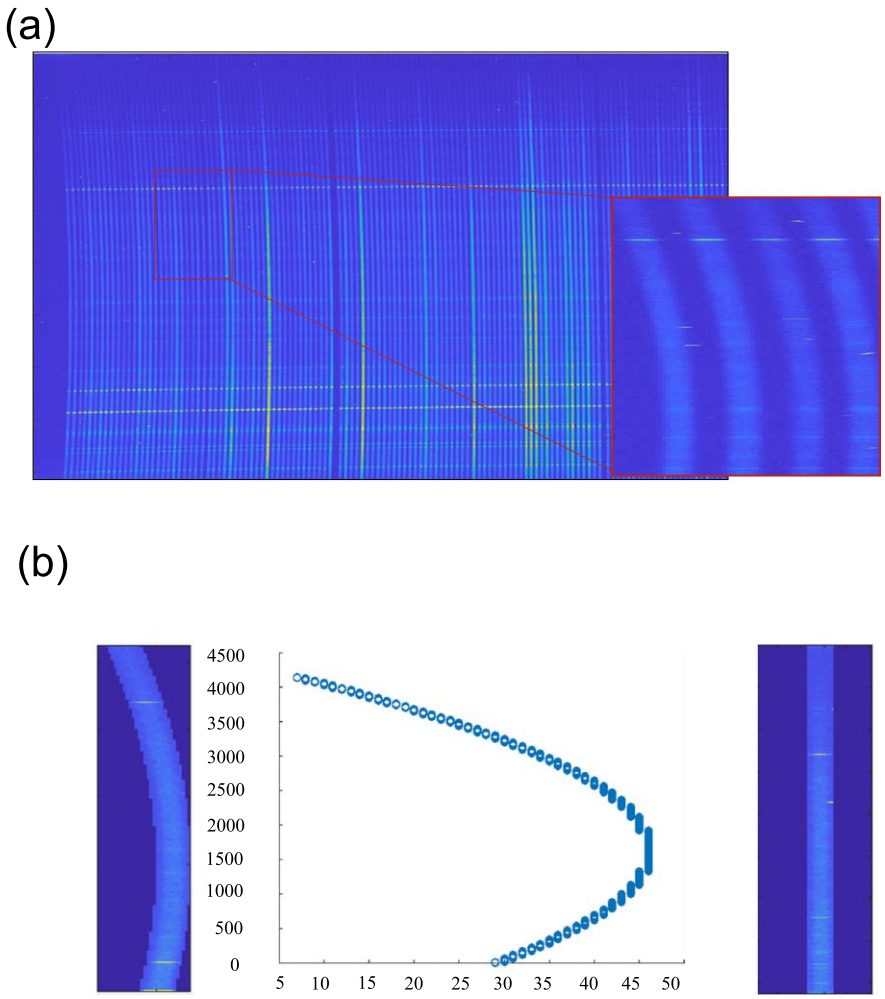

Figure 12. Subpixel correction effect diagram for LAMOST spectra. (a) LAMOST spectral image. (b) Morphology of LAMOST spectra before and after correction.

assigned weight have a unique solution. This process redistributes pixel values around the center peak without introducing or losing spectral information. Summing the fiber spectra along the wavelength direction shows that the total pixel values for each row remain unchanged before and after correction, preserving the spectral distribution.

Additionally, while spectral intensity is preserved during resampling, the associated errors must also be considered. In astronomical spectral applications, intensity values alone do not fully characterize the spectrum; the errors tied to each intensity value are equally important. These errors stem from sources like photon noise, readout noise, dark current, and background noise. Resampling may alter these errors, particularly when linear interpolation is used, as this method may not be ideal for error propagation, given that errors are typically calculated as the quadratic sum of multiple factors. Therefore, when working with resampled spectral data, careful attention should be given to the potential impact of error propagation.

4.2. Correction Effect of Smile Distortion

To verify the Smile distortion correction, we calculated the fitting differences of four absorption lines. Table 6 shows that the pixel difference of the four absorption lines does not exceed 0.45 pixels, with over 90% of points having a difference below 0.10 pixels. In Figure 10(a), the horizontal axis represents the fiber spectrum sequence, and the vertical axis shows the ordinate of absorption line 1, with the line at 2586.12 representing the center peak ordinate of the first fiber spectrum, which is used as a reference. In the figure, the valley points fluctuate evenly around the average value of 2586.12, which may be due to the Doppler frequency movement of different points on the Sun. Figure 10(b) shows the appearance of the four selected absorption lines after correction.

To verify the Smile distortion correction, we located two very weak absorption lines near the top and bottom image boundary, labeled as absorption lines 5 and 6. The pixel shift

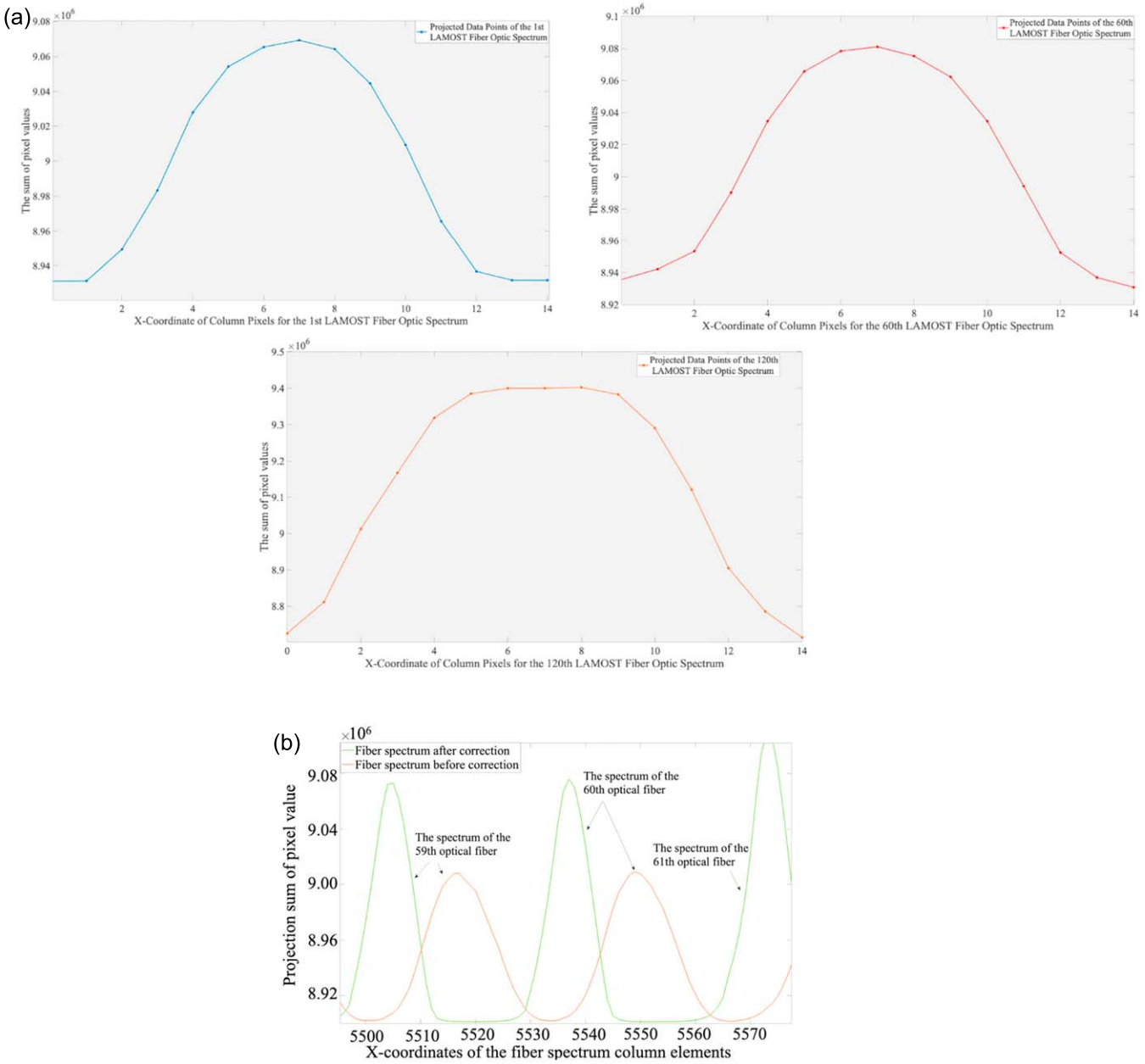

Figure 13. Analysis of LAMOST spectral data processing results. (a) The projection results along the wavelength direction after correction for the 1st, 60th, and 120th LAMOST fiber spectra. (b) The bandwidth variation of the 60th LAMOST fiber spectrum and its two adjacent fiber spectra before and after correction.

differences between absorption lines 5, 6, and line 1 were calculated, as shown in Table 7.

The calculation results are listed in Table 7. The results show that the pixel shifts for absorption lines 5, 6, and 1 are nearly identical, proving that applying the pixel shift from any absorption line to the entire fiber spectrum image is valid. Therefore, we applied the uniform shift from Figure 6(b) to all fiber spectra. The corrected absorption lines 5 and 6 are marked in Figure 10(b).

4.3. Evaluation of the Overall Correction Effect

To show the total effect of Keystone and Smile correction, the leftmost, middle, and rightmost fiber spectra are compared as depicted in Figure 11. Figure 11(a) shows the result of summing the fiber spectra along the wavelength direction, which maps each wavelength to the vertical coordinate of the spectrum image. The *x*-axis represents the vertical coordinate range corresponding to each wavelength in pixels, while the *y*-axis shows the summed

pixel values. We selected wavelength ranges corresponding to vertical coordinates of 1200–1330 pixels, 1610–1710 pixels, and 2550–2950 pixels, and observed the wavelength fluctuations as displayed in Figure 11(b), (c), and (d) respectively. The fluctuations appear random, indicating that the calibration method introduced did not distort the original spectral data, and the original spectral information is well-preserved.

4.4. Instance Verification

To demonstrate the good applicability of the subpixel transformation method, we verified it by processing the LAMOST spectrum shown in Figure 12(a). The spectrum used for validation is obtained from LAMOST which consists of a reflective Schmidt corrector MA (measuring 5.72 m × 4.40 m, made up of 24 hexagonal flat sub-mirrors, each with a diagonal length of 1.1 m and a thickness of 25 mm), a spherical primary mirror MB (measuring 6.67 m × 6.05 m, composed of 37 hexagonal spherical sub-mirrors, each with a diagonal length of 1.1 m and a thickness of 75 mm), and a focal plane. This telescope can observe celestial objects as faint as magnitude 20.5 in an exposure time of 1.5 hr. Since LAMOST is primarily used to observe stars, galaxies, and other celestial objects in the night sky, the overall brightness of these objects is lower than the solar spectral lines observed by FASOT. As a result, there are more noise points in the spectrum. The curvature of the fiber spectral lines is also more noticeable. In Figure 12(a), due to the particularly noticeable curvature in the middle of the fiber spectrum, the x-coordinate value of the farthest lateral pixel of the mth fiber spectrum is greater than the x-coordinate value of the nearest lateral pixel of the $(m+1)$th fiber spectrum. This causes some pixel values of the $(m+1)$th fiber spectrum to be calculated as part of the mth fiber spectrum when summing along the wavelength direction, leading to information distortion. Figure 12(b) illustrates the changes before and after correction for one fiber spectrum. In these figures, the first image shows one of the curved spectral lines from the LAMOST fiber spectrum, the second image presents the result of modeling the center peak points of this spectral line, and the third image shows the result after correction. The fiber spectrum distortion is significant, but after correction, it becomes vertical with pixel points aligned as expected. Statistical analysis shows a maximum pixel deviation of 0.27 pixels, with over 90% of deviations under 0.10 pixels, demonstrating that subpixel shifting effectively corrects most curved spectral lines.

Figure 13(a) shows the projection along the wavelength direction after straightening for the 1st, 60th, and 120th fiber spectra. The figure reveals that the projection shapes of different spectra are inconsistent, indicating non-uniform energy distribution at the fiber output end. This affects the imaging quality of the spectrometer, causing spot distortion and reducing spectral resolution. Non-uniform spot distribution can lead to irregular light intensity distribution on the detector, increasing noise and system errors. The bandwidth variation of the 60th LAMOST fiber spectrum and its two adjacent fiber spectra before and after correction is displayed in Figure 13(b). The figure affirms that the interval between two adjacent peaks increases, and the bandwidth shortens after summing along the wavelength direction. This is caused by the gaps between the fibers during their arrangement, reflecting the true distribution of the spectra. Figures 12 and 13 demonstrate that our subpixel transformation method performs well even with spectral images exhibiting significant line distortion, such as those from LAMOST.

5. Conclusion

A subpixel transformation method was used to precisely correct Keystone and Smile distortion in the two-dimensional spectroscopic images obtained from FASOT observations. After applying the peak-search approach and quartic-polynomial-function fitting, Keystone distortion was corrected, restoring the envelope of the optical fiber output end. Subsequently, the valley-search approach and quartic-polynomial-function fitting were employed to correct Smile distortion, revealing wavelength fluctuations indicating red or blueshifts in the spectrum due to factors such as the Doppler Effect. This subpixel transformation method demonstrates high applicability for correcting various astronomical spectra, including those from instruments like LAMOST.

Funding

Astronomy Joint Research Fund supported this work under cooperative agreements between the National Natural Science Foundation of China (NSFC) and the Chinese Academy of Sciences (CAS) (project numbers: U2031132 and U1931206).

Disclosures

The authors declare no conflicts of interest.

Data Availability Statement

Data underlying the results presented in this paper are not publicly available at this time but may be obtained from the authors upon reasonable request.

References

Bai, H., Su, D.-Q., Liang, M., et al. 2021, RAA, 21, 132
Böker, T., Arribas, S., Lützgendorf, N., et al. 2022, A&A, 661, A82
Cui, X.-Q., Zhao, Y.-H., Chu, Y.-Q., et al. 2012, RAA, 12, 1197
Hong, J., Kim, Y., Choi, B., et al. 2017, OE, 25, 20340
Infante-Sainz, R., Trujillo, I., & Román, J. 2020, MNRAS, 491, 5317
Johnson, T. P., Sasian, J., & Cook, L. G. 2020, AO, 59, G175
Koloniatis, K., Andronis, V., & Karathanassi, V. 2020, Hyperspectral Remote Sensing, 23 (Amsterdam: Elsevier)
Leung, M. C., Chen, S., & Jurgenson, C. 2022, Proc. SPIE, 12188, 1283
Lidman, C., Tucker, B., Davis, T., et al. 2020, MNRAS, 496, 19
Ozaki, S., Fukushima, M., Iwashita, H., et al. 2020, PASJ, 72, 97
Qu, Z. 2011, in ASP Conf. Ser. 437, Solar Polarization 6, ed. J. R. Kuhn (San Francisco, CA: ASP), 423
Smee, S. A., Gunn, J. E., Uomoto, A., et al. 2013, AJ, 146, 32
Zhang, X., Li, X., & Tang, X. 2022, JOptT, 89, 262